Journal of Power Sources 196 (2011) 10169–10175

Contents lists available at ScienceDirect

Journal of Power Sources

journal homepage: www.elsevier.com/locate/jpowsour

Synthesis and electrochemical properties of Na-doped $Li_3V_2(PO_4)_3$ cathode materials for Li-ion batteries

Quan Kuang[a], Yanming Zhao[a,b,*], Zhiyong Liang[a]

[a] School of Materials, South China University of Technology, Guangzhou 510640, PR China
[b] School of Physics, South China University of Technology, Guangzhou 510640, PR China

ARTICLE INFO

Article history:
Received 30 January 2011
Received in revised form 8 July 2011
Accepted 9 August 2011
Available online 16 August 2011

Keywords:
Li-ion batteries
Cathode materials
Lithium vanadium phosphate
Na doping
Sol–gel method

ABSTRACT

Na-doped $Li_{3-x}Na_xV_2(PO_4)_3$/C (x = 0.00, 0.01, 0.03, and 0.05) compounds have been prepared by using sol–gel method. The Rietveld refinement results indicate that single-phase $Li_{3-x}Na_xV_2(PO_4)_3$/C with monoclinic structure can be obtained. Among three Na-doped samples and the undoped one, $Li_{2.97}Na_{0.03}V_2(PO_4)_3$/C sample has the highest electronic conductivity of 6.74×10^{-3} S cm^{-1}. Although the initial specific capacities for all Na-doped samples have no much enhancement at the current rate of 0.2 C, both cycle performance and rate capability have been improved. At the 2.0 C rate, $Li_{2.97}Na_{0.03}V_2(PO_4)_3$/C presents the highest initial capacity of 118.9 mAh g^{-1} and 12% capacity loss after 80 cycles. The partial substitution of Li with Na (x = 0.03) is favorable for electrochemical rate and cyclic ability due to the enlargement of $Li_3V_2(PO_4)_3$ unit cells, optimizing the particle size and morphology, as well as resulting in a higher electronic conductivity.

1. Introduction

The applications of Li-ion batteries in portable electronic products and implantable medical devices have achieved great success up to now. In the near future, Li-ion batteries will come into practical use as power sources of electric vehicles (EVs) and hybrid electric vehicles (HEVs), which require the cathode active materials having even larger energy density, higher output power and better safety performance. In comparison with layered transition metal oxides $LiMO_2$ (M = Co, Ni, Mn), lithium transition metal phosphates $Li_xM_y(PO_4)_z$ with strong P–O bonds and three-dimension solid framework can guarantee both dynamic and thermal stability to meet the need of safety performance in EVs and HEVs. With doping in the bulk, coating at the surface, or reducing the path length by using nano-sized materials, the lithium iron phosphate $LiFePO_4$ has been recognized as the first choice of positive electrode materials for power Li-ion batteries by many battery manufacturers [1–5]. In the family of lithium transition metal phosphates, monoclinic $Li_3V_2(PO_4)_3$ has the highest theoretical specific capacity of 197 mAh g^{-1} in the instance of all the three Li ions can be reversibly extracted from and then reinserted into the host. Besides, $Li_3V_2(PO_4)_3$ with higher electronic conductivity, ionic diffusion coefficient, energy density and discharge voltage compared with $LiFePO_4$, is also considered as a promising cathode material for Li-ion batteries in high-power applications [6]. The $Li_3V_2(PO_4)_3$-based cathode materials are capable to function at the potential up to 4.8 V or even higher, which makes them especially attractive for high-energy applications.

For commercial utilization of Li-ion batteries in high-power field, favorable conductivities for both Li-ion and electron are prerequisite conditions, and it is obvious that pristine $Li_3V_2(PO_4)_3$ is far away from these requirements. Although after optimizing solid-state synthesis routine [7], bare $Li_3V_2(PO_4)_3$ revealed the initial discharge capacity of 146.3 mAh g^{-1} in the voltage of 3.0–4.8 V, but rather poor cycle performance (75.4% of the initial capacity after 50 cycles) owing to its low electronic conductivity. However, carbon-coated $Li_3V_2(PO_4)_3$ composites exhibited much better cycle performance (137.5 mAh g^{-1} at 50th cycle, 94.6% of initial discharge capacity) [7]. Apart from the unremitting efforts via carbon coating with a variety of carbon sources [7–10], it is more preferable to dope $Li_3V_2(PO_4)_3$ with trace elements to improve its intrinsic properties without degrading its energy density. On one hand, V-site substitutions of $Li_3V_2(PO_4)_3$ by Ti^{4+} [11], Zr^{4+} [12], Fe^{3+} [13], Al^{3+} [14,15], Cr^{3+} [16], Sc^{3+} [17], Mg^{2+} [18,19] and Co^{2+} [20] have been extensively explored. The reversible capacity and cycle performance have been enhanced in some cases. On the other hand, Li^+ substituted by K^+ in $Li_3V_2(PO_4)_3$ has been investigated by Mateyshina and Uvarov recently [17], and he found that the samples doped with

* Corresponding author. Tel.: +86 20 87111963; fax: +86 20 87112837.
E-mail address: zhaoym@scut.edu.cn (Y. Zhao).

0378-7753/$ – see front matter © 2011 Elsevier B.V. All rights reserved.
doi:10.1016/j.jpowsour.2011.08.044

potassium exhibited flat charge/discharge curves but worse cycle ability. However, sodium doped monoclinic $Li_3V_2(PO_4)_3$ has never been reported yet.

Na-doped cathode materials have been investigated by using computational and experimental methods. Sun and co-workers prepared layered $Li_{1.1-x}Na_x[Ni_{0.2}Co_{0.3}Mn_{0.4}]O_2$ by sol–gel method, and found that the Na-doped electrodes exhibited superior rate capability and good capacity retention [21]. Chen and co-workers had investigated the electronic structure and ionic dynamic properties of Na-doped $LiFePO_4$ through the first-principle calculations. The calculated results showed that, in comparison with pure $LiFePO_4$, the band gap of Na-doped $LiFePO_4$ was much narrower, and the energy barriers for Li diffusion were decreased [22]. Huang et al. synthesized $Li_{1-x}Na_xFePO_4$/C samples by in situ polymerization restriction-carbon thermal reduction method, and the experimental evidences revealed that the charge transfer resistance of the sample decreased greatly by doping an appropriate amount of sodium [23].

$Li_3V_2(PO_4)_3$ belongs to rhombohedral NASICON phase with S.G. (space group) *Rc* or monoclinic system with S.G. $P2_1/n$ [24]. Rhombohedral phase $Li_2NaV_2(PO_4)_3$ had been prepared by Cushing via ion exchange from $Na_3V_2(PO_4)_3$, and it exhibited a specific discharge capacity of ~96 mAh g^{-1} near 3.7 V versus lithium metal [25]. However, doping the monoclinic $Li_3V_2(PO_4)_3$ with a low content of sodium has not been reported until now. Na-doped monoclinic $Li_3V_2(PO_4)_3$ is expected, as Na-doped $LiFePO_4$, to have better rate ability and cycle performance. For monoclinic $Li_3V_2(PO_4)_3$ compound, there are three Li positions Li1(4e), Li2(4e) and Li3(4e) in the framework [6]. Thus, Li^+ substituted by Na^+ in $Li_3V_2(PO_4)_3$ is much more complicated and fascinating than that in $LiFePO_4$. Hence, in this study, monoclinic $Li_{3-x}Na_xV_2(PO_4)_3$/C (x = 0.00, 0.01, 0.03, and 0.05) composites are first prepared via sol–gel routine, and their electrochemical properties are investigated.

2. Experimental

Conventional solid-state reaction [12–14,17,19,20] and sol–gel [11,15,16,18] methods are two of the most common preparation methods to dope $Li_3V_2(PO_4)_3$ as cathode materials for Li-ion batteries. Compared with solid-state reaction method, sol–gel method has the enormous advantage of producing homogenous mixing of the starting ingredients at atomic level. In order to obtain a series of more homogeneous Na-doped $Li_3V_2(PO_4)_3$ even in a very low Na-doping concentration, the $Li_{3-x}Na_xV_2(PO_4)_3$/C (x = 0.00, 0.01, 0.03, and 0.05) composites were synthesized via the sol–gel method. Stoichiometric amounts of Li_2CO_3, V_2O_5, $NH_4H_2PO_4$, Na_2CO_3 and citric acid were employed as the starting materials. Citric acid was added in the same molar magnitude with V_2O_5 as both chelating reagent and carbon source in the sol–gel process. First, $NH_4H_2PO_4$ and citric acid were dissolved in appropriate amount of deionized water. Then, V_2O_5 powders were added into the colorless solution with magnetic stirring. After a clear orange solution formed, a mixture of Li_2CO_3 and Na_2CO_3 was added to the solution while stirring at 60 °C in a thermostatic water bath to make sure all the carbonates were dissolved. The solution was heated gently with continuous stirring to remove the excess water at 80 °C, and then the solution slowly became a sol. The color of the sol changed from blue to deep blue during heating process. After drying at 80 °C in an air oven, the gel was decomposed at 350 °C for 5 h in an atmosphere of 70% Ar + 30% H_2 in quartz tube furnace to expel H_2O and NH_3. The precursor was reground for 30 min and pressed into pellets of 10 mm in diameter, then sintered at 750 °C for 10 h under the same ambience. The carbon content of the final product was verified by Vario EL (Elementar, Germany) CHNS elemental analyzer.

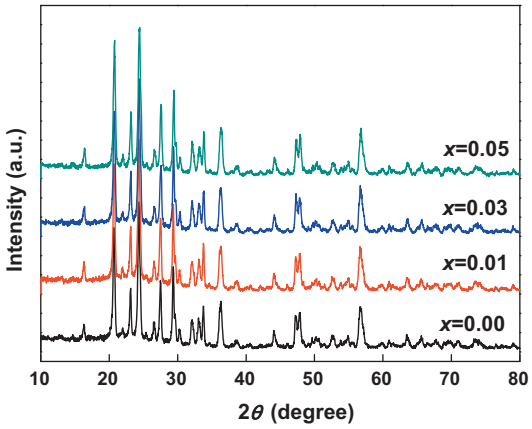

Fig. 1. XRD profiles of $Li_{3-x}Na_xV_2(PO_4)_3$/C (x = 0.00, 0.01, 0.03, and 0.05).

The phase identification of the $Li_{3-x}Na_xV_2(PO_4)_3$/C composites was carried out by X-ray diffraction (XRD) using a Tongda TD-3500 diffractometer with Cu Kα radiation. A graphite monochromator was used for diffracted beams. A step scan mode was adopted with a scanning step of 0.02°. The diffraction intensity data for Rietveld refinement analysis were collected by an MXP 18A-HF diffractometer with rotating anode, which had an 18 kW X-ray generator and Cu Kα radiation. A graphite monochromator was used for diffracted beams. A step scan mode was adopted with a scanning step of 0.02° and a sampling time of 3 s. SEM images were carried out with Nova NanoSEM 430 (Holland FEI) scanning electron microscopy (SEM). The electronic conductivity measurement of $Li_{3-x}Na_xV_2(PO_4)_3$/C powders was adopted with a RTS-8 linear four-point probe measurement system. The specimens used for electronic conductivity measurement were disk-shaped pellets with 10 mm in diameter and 1.5 mm in thickness.

The electrochemical characterizations of $Li_{3-x}Na_xV_2(PO_4)_3$/C powders as cathodes were measured by using a Land CT2001A battery tester (Land®, China). The cathodes of the two-electrode electrochemical cells were fabricated by blending the powders with acetylene black and polyvinylidine fluoride (PVDF) binders in a weight ratio of 80:10:10 in N-methyl-2-pyrrolidone (NMP). The obtained slurry was coated on Al foils, dried at 90 °C for 12 h and pressed at the pressure of 5 MPa. The fabricated electrodes were dried again at 90 °C for 12 h in a vacuum. Two-electrode electrochemical cells were assembled in a Mikrouna® glove box filled with high-purity argon where the lithium metal foils were used as anodes, Celgard® 2320 as separators, and 1 M $LiPF_6$ in EC:DMC (1:1, vol.%) as electrolyte. The electrochemical capacity measurements were performed in the voltage range between 3.0 and 4.8 V, and the electrochemical specific capacity of samples was evaluated on the active materials. The cells were cycled at a current rate of 0.2 C, 0.5 C, 1.0 C, or 2.0 C related to the theoretical capacity of pristine $Li_3V_2(PO_4)_3$ of 197 mAh g^{-1}. For example, the 0.2 C rate means fully charging the theoretical capacity of $Li_3V_2(PO_4)_3$ in 5 h at a current density of 39.4 mA g^{-1}.

3. Results and discussion

In order to investigate the influences of Na-doping on the structure of $Li_3V_2(PO_4)_3$, X-ray diffractions have been performed on $Li_{3-x}Na_xV_2(PO_4)_3$/C (x = 0.00, 0.01, 0.03, and 0.05) composites, as shown in Fig. 1. The XRD peaks of all the samples can be indexed by using Dicvol program [26], and no other impurities were detected within the resolution of our diffractometer. The indexing results (not shown here) indicate that, as expectation, the $Li_{3-x}Na_xV_2(PO_4)_3$/C compounds remain monoclinic structure

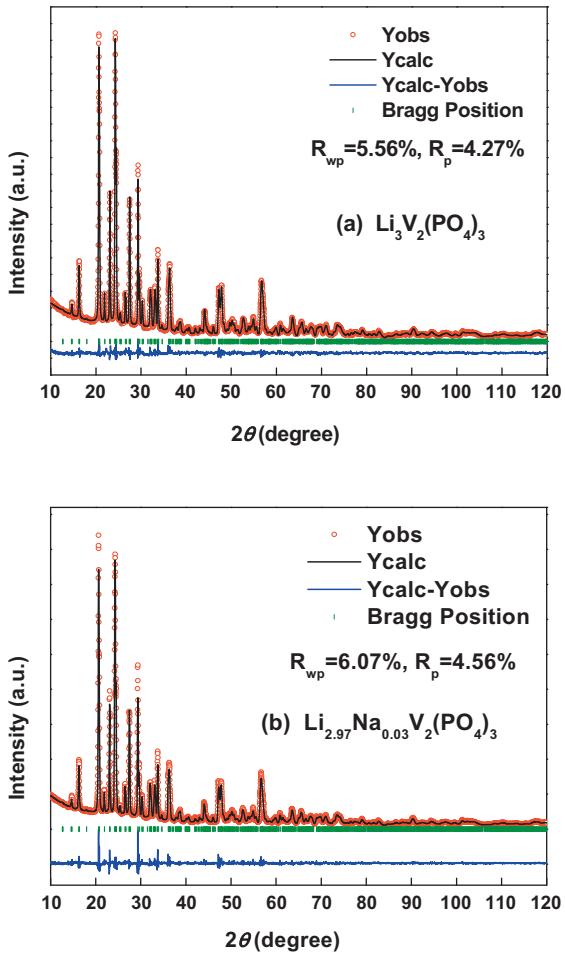

Fig. 2. High-power XRD and Rietveld refinement profiles of (a) $Li_3V_2(PO_4)_3$ and (b) $Li_{2.97}Na_{0.03}V_2(PO_4)_3$.

(S.G. $P2_1/n$) at a low concentration of Na doping although the phase of $Na_3V_2(PO_4)_3$ belongs to trigonal system (S.G. *Rc*) [27], and the single-phase region of the $Li_{3-x}Na_xV_2(PO_4)_3$/C at the poor sodium concentration range determined by X-ray diffraction can be expressed as $0 \le x \le 0.05$. The content of the residual carbon is 6.5 wt% in the final products by element analysis, and the carbon should be amorphous since no other peaks attributed to crystalline carbon can be detected in our XRD patterns.

So as to obtain further information about the fine structure of Na-doped $Li_{3-x}Na_xV_2(PO_4)_3$/C compounds, Rietveld refinements were performed with monoclinic $P2_1/n$ space group (No. 14) (Fig. 2). The reasonably small R_p and R_{wp} factors of the Rietveld refinements shown in Fig. 2 for $Li_3V_2(PO_4)_3$ and $Li_{2.97}Na_{0.03}V_2(PO_4)_3$ reveal that single phase $Li_3V_2(PO_4)_3$ and $Li_{2.97}Na_{0.03}V_2(PO_4)_3$ can be obtained under our experimental conditions. In $Li_3V_2(PO_4)_3$ structure, three lithium atoms per molecular formula occupy three nonequivalent Wyckoff positions Li1(4e), Li2(4e) and Li3(4e) [6]. Li ions in Li3(4e) sites with the highest energy among the three positions are first extracted during charge process based on bond-sum calculation, neutron diffraction and ^{7}Li solid-state NMR [28]. Consequently, for the low concentration of Na-doping in our experiment, Na ions prefer to entering the Li3(4e) position during the synthesis of $Li_{3-x}Na_xV_2(PO_4)_3$ system. In fact, during the refinements of the X-ray diffraction data of $Li_{3-x}Na_xV_2(PO_4)_3$/C compounds (especially for $x = 0.05$) by assuming that Na occupied Li1(4e) or Li2(4e) position, the negative thermal parameters or extraordinarily large *R* factors (R_p and R_{wp}) were obtained. This may be understood here from the difference of ionic radius (Li^+: 0.76 Å and Na^+: 1.02 Å) in the six-fold coordination environment [29]. In the unit cell of $Li_3V_2(PO_4)_3$, no special positions exist, and all of 80 atoms (Li, V, P, and O) occupy Wyckoff positions 4e with different general coordinates (*x*, *y*, *z*). When Na^+ ions enter the different positions (Li1(4e), Li2(4e), or Li3(4e)), it can result in the change of all the general coordinates of V sites (V1(4e) or V2(4e)), P sites (P1(4e)–P3(4e)), as well as O sites (O1(4e)–O8(4e)) due to the difference of ionic radius. Our refinement results reveal that Na^+ ions show a strong preference for occupying the Li3(4e) positions in $Li_{3-x}Na_xV_2(PO_4)_3$/C system.

The lattice parameters together with significant distances in the structure of $Li_{3-x}Na_xV_2(PO_4)_3$ ($x = 0.00$, 0.01, 0.03, and 0.05) from the Rietveld refinement results are given in Table 1. The lattice parameters of $Li_{2.97}Na_{0.03}V_2(PO_4)_3$ are $a = 8.6093(4)$ Å, $b = 8.6028(3)$ Å $c = 12.0492(5)$ Å, $\beta = 90.532(2)^\circ$, and $V = 892.38(9)$ Å^3, which are larger than that of $Li_3V_2(PO_4)_3$. The lattice constants *a*, *b*, and *c* axis of $Li_{3-x}Na_xV_2(PO_4)_3$ increase nearly linearly by 18.2%, 3.2% and 20.8% per substituted sodium, respectively, which can be a clue illustrating the Na ions allocated in the $Li_3V_2(PO_4)_3$ lattice. The lithium-ion hopping processes primarily depend on the activation energies of Li ions in different equivalent sites. Cahill et al. found that the activation energies were correlated directly to the interatomic Li–Li distances and the closest Li–O contacts [30]. Both short Li–Li distances and slack Li–O contacts can lead to low Li activation energy and then, improve the ionic conductivity within metal phosphates. Table 1 also reveals the interatomic Li–Li distances and the closest Li–O contacts among three nonequivalent Wyckoff positions Li1(4e), Li2(4e) and Li3(4e) in $Li_{3-x}Na_xV_2(PO_4)_3$ ($x = 0.00$, 0.01, 0.03, and 0.05) unit cells. Although the Li2–Li3 distance increases with Na doping content, the interatomic distances of Li1–Li2 (3.21(6) Å) and Li1–Li3 (3.32(5) Å) of $Li_{2.97}Na_{0.03}V_2(PO_4)_3$ are shorter than that of the pristine $Li_3V_2(PO_4)_3$. Besides, the closest Li–O contacts of $Li_{2.97}Na_{0.03}V_2(PO_4)_3$ in three distinct Li sites, ranging from 1.83 to 1.98 Å, become wider than that of the undoped one. Thus, it is expected that short Li–Li distances and slack Li–O contacts, com-

Table 1
Rietveld refinement results of $Li_{3-x}Na_xV_2(PO_4)_3$ (short for $Li_{3-x}Na_xVP$, $x = 0.00$, 0.01, 0.03, and 0.05) with monoclinic $P2_1/n$ space group (No. 14).

Compounds		Li_3VP	$Li_{2.99}Na_{0.01}VP$	$Li_{2.97}Na_{0.03}VP$	$Li_{2.95}Na_{0.05}VP$
a (Å)		8.6037(3)	8.6052(3)	8.6093(4)	8.6128(3)
b (Å)		8.6019(3)	8.6023(3)	8.6028(3)	8.6035(3)
c (Å)		12.0430(4)	12.0448(4)	12.0492(5)	12.0534(5)
β(deg)		90.523(2)	90.473(2)	90.532(2)	90.662(2)
V (Å^3)		891.24(5)	891.58(5)	892.38(7)	893.10(6)
Li1–Li2 (Å)		3.33(4)	3.28(5)	3.21(6)	3.12(5)
Li1–Li(Na)3 (Å)		3.49(4)	3.43(4)	3.32(5)	3.19(4)
Li2–Li(Na)3 (Å)		2.98(4)	3.06(5)	3.31(5)	3.54(4)
Closest Li–O contact (Å)	Li1–O	1.80(3)	1.82(3)	1.83(4)	1.86(3)
	Li2–O	1.95(3)	1.96(3)	1.98(4)	2.01(3)
	Li(Na)3–O	1.91(3)	1.92(3)	1.91(3)	1.92(3)

Table 2
Electronic conductivities of $Li_{3-x}Na_xV_2(PO_4)_3$/C (x = 0.00, 0.01, 0.03, and 0.05) with different content of sodium by linear four-point probe measurement.

Compounds	$Li_3V_2(PO_4)_3$	$Li_{2.99}Na_{0.01}V_2(PO_4)_3$	$Li_{2.97}Na_{0.03}V_2(PO_4)_3$	$Li_{2.95}Na_{0.05}V_2(PO_4)_3$
Conductivity ($S\,cm^{-1}$)	2.16×10^{-4}	1.67×10^{-3}	6.74×10^{-3}	4.72×10^{-3}

pared with $Li_3V_2(PO_4)_3$, can benefit the diffusion of Li ions within the Na-doped $Li_{2.97}Na_{0.03}V_2(PO_4)_3$ framework.

As shown in Table 2, the electronic conductivity of pristine $Li_3V_2(PO_4)_3$ from the four-point probe measurement agrees well with the previous works [16,20]. There is more than one order of magnitude improvement in electronic conductivity even with such a low level of Na doping. It is noteworthy that $Li_{2.97}Na_{0.03}V_2(PO_4)_3$ has the highest electronic conductivity of $6.74 \times 10^{-3}\,S\,cm^{-1}$ among the four samples. The effective radius of Na^+ ion (1.02 Å) in six-coordination environment is much larger than that of Li^+ ion (0.76 Å) [29]. Like the Na-doped $LiFePO_4$ system [22], the Na doping thus expands the lattices of $Li_3V_2(PO_4)_3$ and leads to distortion of V positions, thus results in narrowing the band gap. Therefore, Na doping can enhance the electronic conductivity of $Li_3V_2(PO_4)_3$.

The 1st cycle charge–discharge curves of the $Li_{3-x}Na_xV_2(PO_4)_3$/C (x = 0.00, 0.01, 0.03, 0.05) samples at 0.2 C rate in the voltage range of 3.0–4.8 V are shown in Fig. 3, where the electrochemical behavior of the undoped $Li_3V_2(PO_4)_3$/C material is well consistent with previously reported result [7]. It exhibits four charge voltage plateaus (3.60 V, 3.68 V, 4.09 V, and 4.53 V) and three discharge voltage plateaus (4.02 V, 3.64 V, 3.58 V) in our experiment, which are relative to a sequence of transition processes between the single phases $Li_{3-y}V_2(PO_4)_3$: y = 0.0, 0.5, 1.0, 2.0, and 3.0 [28]. In the cases of V^{3+} substituted by Ti^{4+}, Zr^{4+}, Cr^{3+} or Mg^{2+} in $Li_3V_2(PO_4)_3$, the first two charge plateaus were gradually merged into one and became more sloped [11,12,16,18,19]. It had been shown that Co-doping can adjust the redox potentials of $Li_3V_2(PO_4)_3$ as well [20]. All of these are mainly caused by the differences of electrochemical activities between V^{3+} and other metallic cations (Ti^{4+}, Zr^{4+}, Cr^{3+}, Mg^{2+} and Co^{2+}). More specifically, both the discharge capacity and cycle performance were enhanced in the Ti-doped $Li_3V_2(PO_4)_3$ system [11], where the first two plateaus present slightly sloping during discharge and the boundary became ambiguous gradually with the increase of Ti-doping content. The ionic conductivity can increase to three orders of magnitudes after doping. The improved conductivity and specific capacity, together with the disappearance of two-plateau boundary in the capacity–voltage profiles can be ascribed to the disorder of Li ions due to additional Li vacancies by the Ti^{4+} doping.

The Zr-doped $Li_3V_2(PO_4)_3$ samples [12] exhibited not only the disappearance of two-plateau boundary in the charge/discharge curves but also the enhancement of discharge capacity. The slightly sloping of two plateaus showed a considerably improved charge/discharge cycle performance compared to that of the pristine one. The neutron diffraction refinement results showed that the enhanced cycle performance came from the disordered Li-ion arrangement in the orthorhombic phase. For the case of Cr-doped $Li_3V_2(PO_4)_3$ [16], the initial capacity decreased monotonically and the charge curves became featureless with increasing Cr-doping content. However, both cycle performance and rate capability had excited improvement with moderate Cr-doping content, which can be attributed to the optimizing particle size, carbon coating quality, and structural stability during the proper amount of Cr-doping (x = 0.1) in V sites. In the situation of Co-doped $Li_3V_2(PO_4)_3$ [20], the voltage peaks associated with the extraction of three Li ions shifted to higher voltages with an increase in Co content, and when the Co-doping content reached 0.15, the peak positions returned to those of the unsubstituted phase. The doping in V sites by Co^{2+} was favorable for the structural stability of $Li_3V_{2-x}Co_x(PO_4)_3$/C compounds and thus counteracted the volume changes during the reversible Li^+ extraction/insertion, resulting in improved cycling ability.

Compared with the Ti^{4+}, Zr^{4+}, Cr^{3+}, Mg^{2+} and Co^{2+} doping in V-site of $Li_3V_2(PO_4)_3$, the profiles of charge–discharge curves for different Na content samples (Fig. 3) are almost the same, and no distinct enhancement or degeneracy of voltage plateaus is observed after Na-doping. Even the polarizations of voltage caused by the impedance of cathode materials are not apparently disparate in such low current density of 39.4 mA g^{-1}. The initial discharge specific capacities for $Li_{3-x}Na_xV_2(PO_4)_3$/C samples with x = 0.00, 0.01, 0.03, and 0.05 are 168, 169.7, 170, and 169.5 mAh g^{-1}, respectively. The results of slight increase of discharge specific capacity in our experiments suggest that Na-doping does not block the tunnels of Li ions to reduce the charge and discharge capacities at low rate. Although the initial discharge specific capacities have no much enhancement at the low charge/discharge rate of 0.2 C, as shown in Fig. 4, the better capacity retention can be obtained after 10 cycles.

Fig. 4 also shows the rate abilities of $Li_{3-x}Na_xV_2$ $(PO_4)_3$/C (x = 0.00, 0.01, 0.03, 0.05) at various charge/discharge rates of 0.2 C,

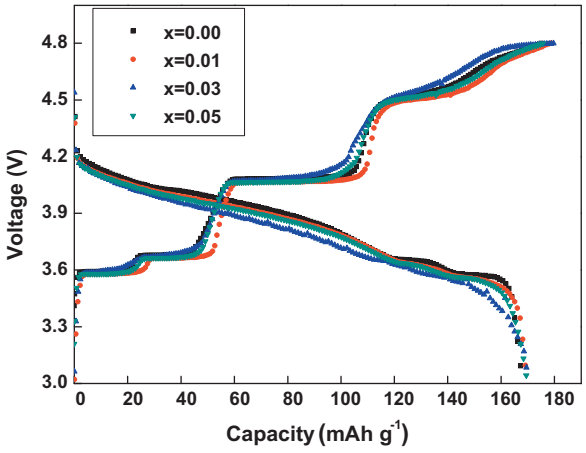

Fig. 3. Charge and discharge curves of $Li_{3-x}Na_xV_2(PO_4)_3$/C (x = 0.00, 0.01, 0.03, 0.05) for the initial cycle at a current density of 0.2 C.

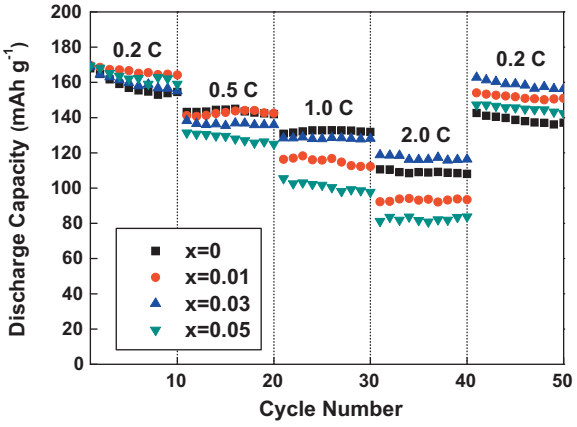

Fig. 4. Rate abilities of $Li_{3-x}Na_xV_2(PO_4)_3$/C (x = 0.00, 0.01, 0.03, 0.05) at various charge/discharge rates of 0.2 C, 0.5 C, 1.0 C, 2.0 C, and finally 0.2 C in succession.

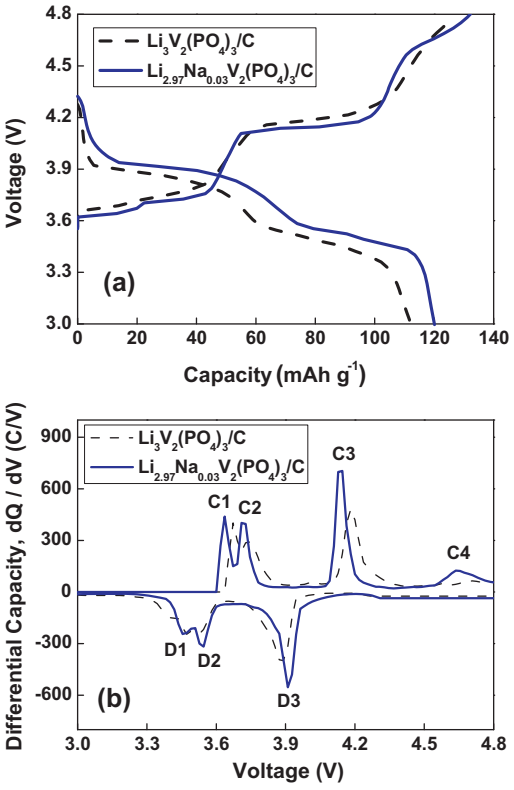

Fig. 5. (a) Charge–discharge curves and (b) differential capacity data of $Li_3V_2(PO_4)_3$/C and $Li_{2.97}Na_{0.03}V_2(PO_4)_3$/C for the initial cycle at a rate of 2.0 C.

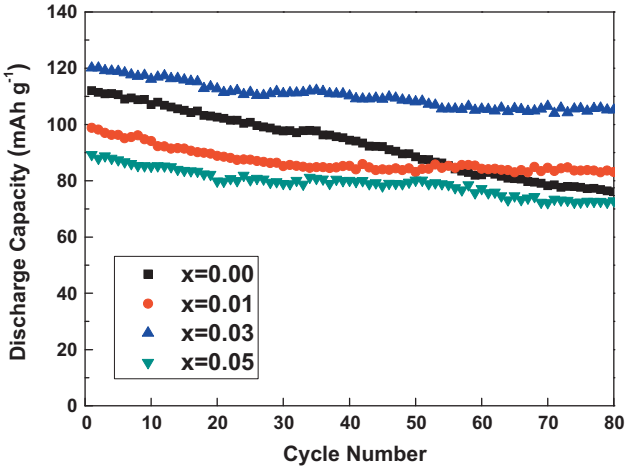

Fig. 6. Cycle performances of $Li_{3-x}Na_xV_2(PO_4)_3$ (x = 0.00, 0.01, 0.03, 0.05) at 2.0 C rate.

0.5 C, 1.0 C, 2.0 C, and finally 0.2 C in succession. The better capacity retentions of Na-doped samples are mainly attributed to the pillar effect of Na ions where, as suggested by Park et al. [21] in $Li_{1.1}Ni_{0.2}Co_{0.3}Mn_{0.4}O_2$ and Yin et al. in $LiFePO_4$ [23] respectively, the sodium ions might be acted as pillars in $Li_{3-x}Na_xV_2(PO_4)_3$ structures. This kind of pillars in the $Li_{3-x}Na_xV_2(PO_4)_3$ framework can provide larger space for the movement of lithium ions which agrees with our XRD results of increasing the unit cell volume of $Li_{3-x}Na_xV_2(PO_4)_3$ with Na content (Table 1) and thus, enhances the ionic conductivity as well as the Li^+ diffusion coefficient. At the higher charge/discharge rates (0.5 C, 1.0 C and 2.0 C), the electrochemical performances are closely related to the electronic and

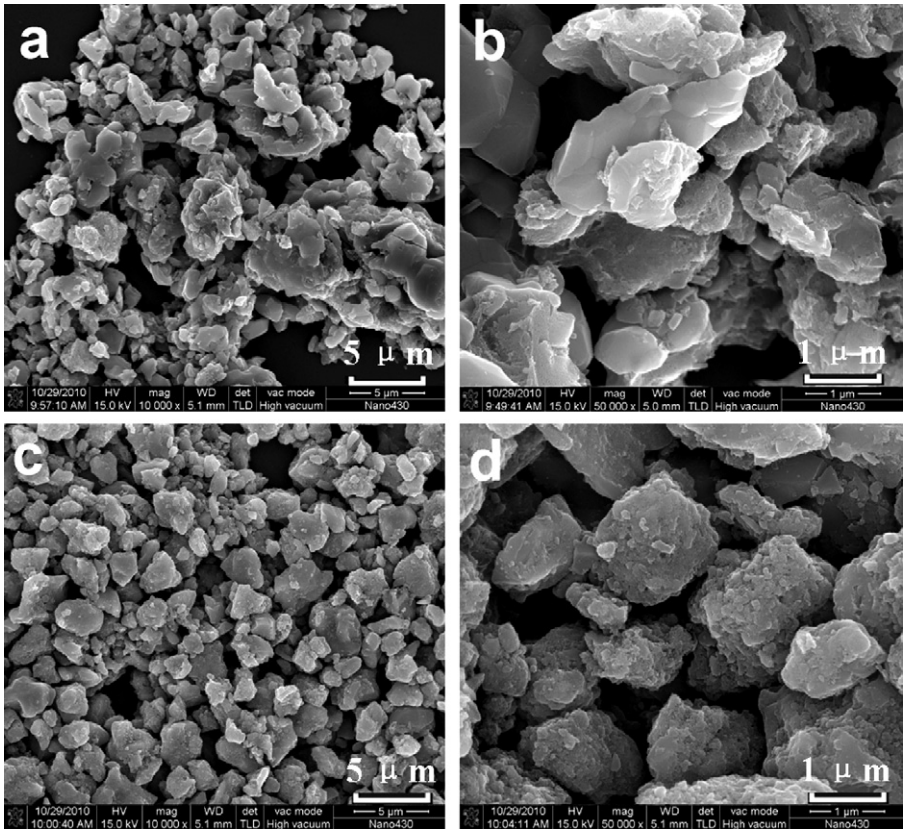

Fig. 7. SEM images of (a) and (b) $Li_3V_2(PO_4)_3$, and (c) and (d) $Li_{2.97}Na_{0.03}V_2(PO_4)_3$.

ionic conductivities of cathode materials [31], and depend on the slower process between electronic and ionic transportations. In the cases of 0.5 C and 1.0 C, all the Na-doped samples export less discharge specific capacities than the undoped one. These are mainly due to the exotic Na ions which obstruct the diffusion of Li ions at higher rate, sequentially Li ions have not enough time to transport from the interior of cathode particles into the electrolyte. This cannot be found at low rate of 0.2 C, because there is sufficient time for Li ions to bypass the Na ions and continue diffusing at low current circumstance. When the charge/discharge rate came to 2.0 C, the electrochemical performance of $Li_{3-x}Na_xV_2(PO_4)_3$/C system began to have more connection with the electronic conductivity. $Li_{2.97}Na_{0.03}V_2(PO_4)_3$ with the highest electronic conductivity of 6.74×10^{-3} S cm^{-1} as shown in Table 2, has the highest discharge capacity of 118.9 mAh g^{-1} among the four samples. The large capacity gap (~20 mAh g^{-1}) of undoped $Li_3V_2(PO_4)_3$ between 1.0 C and 2.0 C can be ascribed to its relatively poor electronic conductibility. Although the doped sample with $x = 0.05$ has higher electronic capacity compared to undoped $Li_3V_2(PO_4)_3$, the blocking effect of $Li_{2.95}Na_{0.05}V_2(PO_4)_3$ is the most serious, which leads to the worst discharge capacity. After 40 cycles through four different charge/discharge rates (0.2 C, 0.5 C, 1.0 C, and 2.0 C in order), the batteries were finally tested at a rate of 0.2 C again. All the Na-doped $Li_{3-x}Na_xV_2(PO_4)_3$/C ($x = 0.01$, 0.03, 0.05) exhibit better discharge capacity than that of the undoped one. Even though the $Li_{2.95}Na_{0.05}V_2(PO_4)_3$, with the worst discharge capacity of 80 mAh g^{-1} at high rate, can easily recover the capacity of 145 mAh g^{-1} at the last cycle with 0.2 C rate. The $Li_{2.97}Na_{0.03}V_2(PO_4)_3$ material has the highest discharge capacity of 156.5 mAh g^{-1} in the last cycle (~92% capacity of initial cycle), while the capacity reservation rate of pure $Li_3V_2(PO_4)_3$ is only 82%. These improvements of Na-doped $Li_3V_2(PO_4)_3$ are basically profited from their enhanced electronic conductivities and the pillar effect of Na ions. So far as we know, moderate Na^+ doping in the Li sites of monoclinic $Li_3V_2(PO_4)_3$ can improve the electronic conductivity and rate ability like the cases of V sites doping with Al^{3+} [15], Cr^{3+} [16], and Mg^{2+} [19] ions.

Although the voltage plateaus have no evidently difference for the doped and undoped $Li_3V_2(PO_4)_3$ at the low charge/discharge rate of 0.2 C (Fig. 3), significant distinction of voltage polarization between charge and discharge can be observed of $Li_3V_2(PO_4)_3$ and $Li_{2.97}Na_{0.03}V_2$ $(PO_4)_3$ at a high rate of 2.0 C, as shown in Fig. 5a. In Fig. 5b, the differential capacity data of $Li_3V_2(PO_4)_3$ and $Li_{2.97}Na_{0.03}V_2(PO_4)_3$ materials show the redox transitions associated with the sequential removal of lithium from the energetically inequivalent sites within the monoclinic structure (peaks C1–C4), and the corresponding lithium-insertion reactions are denoted as peaks D1 through D3. Compared with the undoped $Li_3V_2(PO_4)_3$, the voltage peaks associated with the extractions of three Li^+ from $Li_{2.97}Na_{0.03}V_2(PO_4)_3$ shift to lower voltages by ~50 mV, and the voltage peaks corresponding lithium-insertion reactions are ~30 mV higher than that of $Li_3V_2(PO_4)_3$. It should also be noted that the lithium extraction and insertion processes for the $Li_{2.97}Na_{0.03}V_2(PO_4)_3$ phase are now much more ordered than that of unsubstituted $Li_3V_2(PO_4)_3$, as evidenced by the emergence of relatively more intense and sharper peaks, as depicted in Fig. 5b. The relatively narrow gap of redox peaks and more order of Li^+ extraction/insertion processes suggest that the $Li_{2.97}Na_{0.03}V_2(PO_4)_3$ sample has smaller voltage polarization and better electrochemical reversibility than that of $Li_3V_2(PO_4)_3$. This is consistent with our results shown in Fig. 4, where the specific capacity of $Li_{2.97}Na_{0.03}V_2(PO_4)_3$ measured at the rate of 2.0 C is higher than that of the undoped $Li_3V_2(PO_4)_3$.

The cycle performances of $Li_{3-x}Na_xV_2(PO_4)_3$/C ($x = 0.00$, 0.01, 0.03, and 0.05) at 2.0 C rate are given in Fig. 6. The electrochemical performances of $Li_{3-x}Na_xV_2(PO_4)_3$/C samples before the 30th cycle are similar to the rate-ability tests shown in Fig. 4. The specific capacities after 80 cycles at 2.0 C can be held at 68%, 84%, 88% and 82% with $x = 0.00$, 0.01, 0.03, and 0.05, respectively. After 80 cycles, all the Na-doped samples have the better cycle performances than that of the undoped $Li_3V_2(PO_4)_3$ as the situations of V-site doping of $Li_3V_{2-x}M_x(PO_4)_3$ (M = Ti [11], Fe [13], Al [14], Co [20], Mg [18]), although $Li_{2.99}Na_{0.01}V_2(PO_4)_3$ and $Li_{2.95}Na_{0.05}V_2(PO_4)_3$ have the relatively low discharge capacity in the primeval cycles. This might be understood here from the pillar effect of Na ions, which also can be found in the Na-doped $Li_{1.1}Ni_{0.2}Co_{0.3}Mn_{0.4}O_2$ [21] and $LiFePO_4$ materials [23]. It should also be noted that $Li_{2.97}Na_{0.03}V_2(PO_4)_3$ exhibits the best discharge capacity and the highest capacity retention rate of 88% in whole 80 cycles, which are attributed to the improvement of electronic conductivity as well as the electrochemical reversibility.

Although monoclinic $Li_3V_2(PO_4)_3$ has been stated as a high rate cathode, in the previous studies it had been reported that the morphology and surface area of obtained particles still have the notable influence on the cycle performance [6]. Here, the SEM images of $Li_3V_2(PO_4)_3$ and $Li_{2.97}Na_{0.03}V_2(PO_4)_3$ powders are compared in Fig. 7. The non-uniform particles which are agglomerated with the particle size of 1–5 μm can also be observed in Fig. 7a and b respectively, where the abundance of grain-boundary leads to poor connection of $Li_3V_2(PO_4)_3$/C particles, which may be responsible for the lower initial capacity than that of Na-doped samples. In contrast, the particles with the relatively uniform shape and the size of ~1 μm for $Li_{2.97}Na_{0.03}V_2(PO_4)_3$/C compound can be observed (Fig. 7c and d). In particles with a larger diameter and a relative lower specific area, the Li ions have to diffuse over greater distance between the surface and center during lithium insertion or extraction, and the active material near the center of particle contributes very little to the charge/discharge reaction [32]. Our experimental results suggest that the better electrochemical performance can be obtained through optimizing the powder characteristic at a moderate Na-doping content. It is expected that this type of morphology which have a relatively larger specific area would be very effective in enhancing the ionic conductivity and thus, leads to relatively large capacity and favorable rate ability of $Li_{2.97}Na_{0.03}V_2(PO_4)_3$/C.

4. Conclusions

Na-doped $Li_{3-x}Na_xV_2(PO_4)_3$/C ($x = 0.00$, 0.01, 0.03, and 0.05) cathode materials have been successfully synthesized by using sol–gel method. The Rietveld refinement results indicate that single-phase $Li_{3-x}Na_xV_2(PO_4)_3$/C materials can be obtained, and the lattice parameters of $Li_{2.97}Na_{0.03}V_2(PO_4)_3$ are larger than that of the undoped one. $Li_{2.97}Na_{0.03}V_2(PO_4)_3$/C sample has the highest electronic conductivity among four samples. The electrochemical properties of $Li_{3-x}Na_xV_2(PO_4)_3$/C have been investigated, and the results show that although the initial specific capacities for all Na-doped samples have no much enhancement at 0.2 C rate, both cycle performance and rate capability have been improved. At the 2.0 C rate, the $Li_{2.97}Na_{0.03}V_2(PO_4)_3$/C presents the highest initial capacity and the lowest capacity loss after 80 cycles. The doping in Li sites by proper amount of Na would be favorable to expanding the lattices and enhancing the electronic conductivity of $Li_{3-x}Na_xV_2(PO_4)_3$/C compounds due to the pillar effect of Na ions. Our results show that $Li_{2.97}Na_{0.03}V_2(PO_4)_3$ has shorten Li–Li distances and widen Li–O contacts, which may result in the improvement of cyclic ability. In otherwise, our SEM results reveal that there are large differences in particle morphology between $Li_{2.97}Na_{0.03}V_2(PO_4)_3$ and $Li_3V_2(PO_4)_3$. Our results suggest that the partial substitution of Li with Na ($x = 0.03$) should be favorable for electrochemical rate and cyclic ability due to the enlargement of $Li_3V_2(PO_4)_3$ unit cells, opti-

mizing the particle size and shape, as well as resulting in a higher electronic conductivity.

Acknowledgments

This work was funded by NSFC Grant (No. 50772039) supported through NSFC Committee of China and the Foundation (No. S2011020000521) supported through the Science and Technology Bureau of Guangdong Government, respectively. The authors are indebted to Prof. C. Dong of Institute of Physics, Chinese Academy of Science for his assistance with the X-ray diffraction experiments.

References

[1] M. Winter, R.J. Brodd, Chem. Rev. 104 (2004) 4245.
[2] M.S. Whittingham, Chem. Rev. 104 (2004) 4271.
[3] H. Li, Z.X. Wang, L.Q. Chen, X.J. Huang, Adv. Mater. 21 (2009) 4593.
[4] J.B. Goodenough, Y. Kim, Chem. Mater. 22 (2010) 587.
[5] B.L. Ellis, K.T. Lee, L.F. Nazar, Chem. Mater. 22 (2010) 691.
[6] H. Huang, S.-C. Yin, T. Kerr, N. Taylor, L.F. Nazar, Adv. Mater. 14 (2002) 1525.
[7] P. Fu, Y.M. Zhao, Y.Z. Dong, X.N. An, G.P. Shen, J. Power Sources 162 (2006) 651.
[8] M.M. Ren, Z. Zhou, X.P. Gao, W.X. Peng, J.P. Wei, J. Phys. Chem. C 112 (2008) 5689.
[9] Y.Z. Li, Z. Zhou, X.P. Gao, J. Yan, Electrochim. Acta 52 (2007) 4922.
[10] X.H. Rui, C. Li, C.H. Chen, Electrochim. Acta 54 (2009) 3374.
[11] S.Q. Liu, S.C. Li, K.L. Huang, Z.H. Chen, Acta Phys. Chim. Sin. 23 (2007) 537.
[12] M. Sato, H. Ohkawa, K. Yoshida, M. Saito, K. Uematsu, K. Toda, Solid State Ionics 135 (2000) 137.
[13] M.M. Ren, Z. Zhou, Y.Z. Li, X.P. Gao, J. Yan, J. Power Sources 162 (2006) 1357.
[14] J. Barker, R.K.B. Gover, P. Burns, A. Bryan, J. Electrochem. Soc. 154 (2007) A307.
[15] B. Zhang, J.Q. Liu, Q. Zhang, Y.H. Li, Trans. Nonferrous Met. Soc. China 20 (2010) 619.
[16] Y.H. Chen, Y.M. Zhao, X.N. An, J.M. Liu, Y.Z. Dong, L. Chen, Electrochim. Acta 54 (2009) 5844.
[17] Y.G. Mateyshina, N.F. Uvarov, J. Power Sources 196 (2011) 1494.
[18] J.S. Huang, L. Yang, K.Y. Liu, Y.F. Tang, J. Power Sources 195 (2010) 5013.
[19] C.S. Dai, Z.Y. Chen, H.Z. Jin, X.G. Hu, J. Power Sources 195 (2010) 5775.
[20] Q. Kuang, Y.M. Zhao, X.N. An, J.M. Liu, Y.Z. Dong, L. Chen, Electrochim. Acta 55 (2010) 1575.
[21] S.-H. Park, S.-S. Shin, Y.-K. Sun, Mater. Chem. Phys. 95 (2006) 218.
[22] C.Y. Ouyang, D.Y. Wang, S.Q. Shi, Z.X. Wang, H. Li, X.J. Huang, L.Q. Chen, Chin. Phys. Lett. 23 (2006) 61.
[23] X.G. Yin, K.L. Huang, S.Q. Liu, H.Y. Wang, H. Wang, J. Power Sources 195 (2010) 4308.
[24] D. Morgan, G. Ceder, M.Y. Saïdi, J. Barker, J. Swoyer, H. Huang, G. Adamson, Chem. Mater. 14 (2002) 4684.
[25] B.L. Cushing, J.B. Goodenough, J. Solid State Chem. 162 (2001) 176.
[26] A. Boultif, D. Louër, J. Appl. Crystallogr. 37 (2004) 724.
[27] I.V. Zatovsky, Acta. Cryst. E66 (2010) i12.
[28] S.-C. Yin, H. Grondey, P. Strobel, M. Anne, L.F. Nazar, J. Am. Chem. Soc. 125 (2003) 10402.
[29] R.D. Shannon, Acta Cryst. A32 (1976) 751.
[30] L.S. Cahill, R.P. Chapman, J.F. Britten, G.R. Goward, J. Phys. Chem. B 110 (2006) 7171.
[31] M. Park, X. Zhang, M. Chung, G.B. Less, A.M. Sastry, J. Power Sources 195 (2010) 7904.
[32] A.S. Andersson, J.O. Thomas, J. Power Sources 97/98 (2001) 498.